JCI The Journal of Clinical Investigation

Methylation of immune synapse genes modulates tumor immunogenicity

Anders Berglund, … , James Mulé, Sungjune Kim

J Clin Invest. 2019. https://doi.org/10.1172/JCI131234.

Concise Communication In-Press Preview Immunology

Graphical abstract

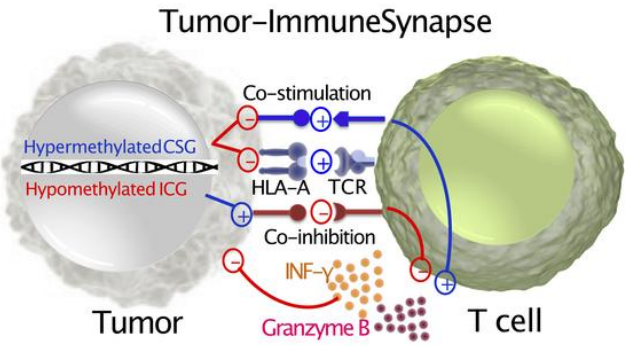

Title: Methylation of immune synapse genes modulates tumor immunogenicity.

AUTHORS

Anders Berglund[1], Matthew Mills[2], Ryan M Putney[1], Imène Hamaidi[3], James Mulé[2,3,4], Sungjune Kim[2,3*]

AFFILIATIONS

Departments of [1]Bioinformatics and Biostatistics, [2]Radiation Oncology, [3]Immunology, [4]Cutaneous Oncology, H. Lee. Moffitt Cancer Center & Research Institute, Tampa, FL 33612

*Correspondence to: 12902 Magnolia Dr, Tampa, FL 33612, USA, Sungjune.kim@moffitt.org

ABSTRACT

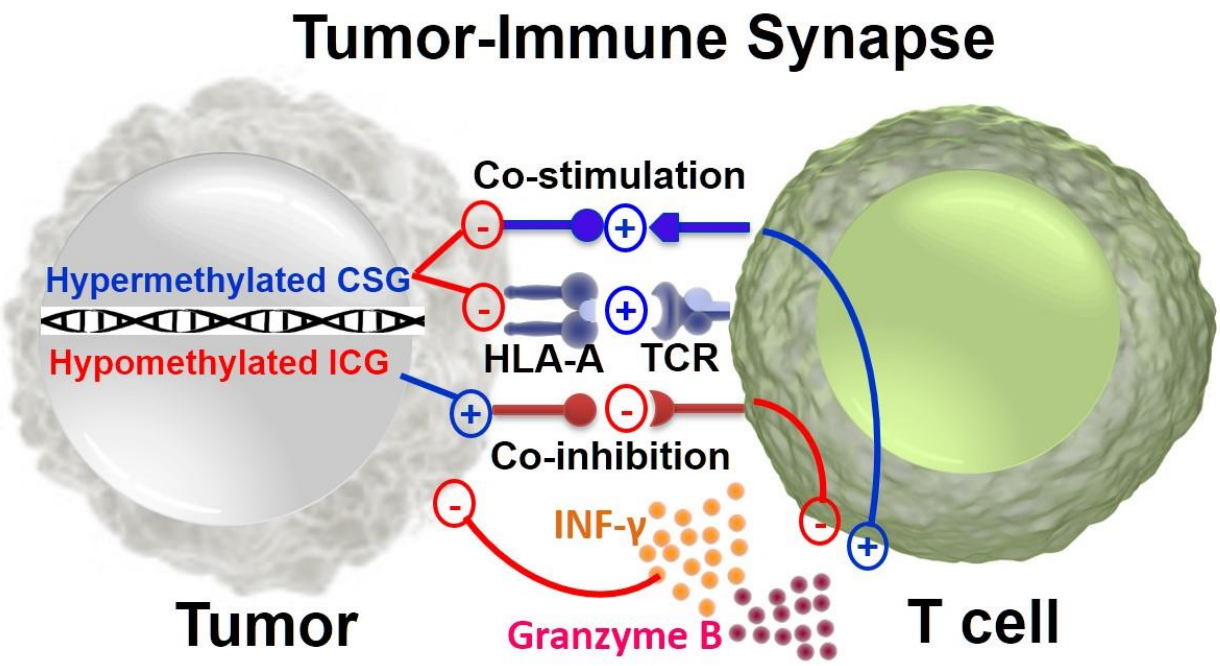

Cancer immune evasion is achieved through multiple layers of immune tolerance mechanisms including immune editing, recruitment of tolerogenic immune cells, and secretion of immune suppressive cytokines. Recent success with immune checkpoint inhibitors in cancer immunotherapy suggests a dysfunctional immune synapse as a pivotal tolerogenic mechanism. Tumor cells express immune synapse proteins to suppress the immune system, which is often modulated by epigenetic mechanisms. When the methylation status of key immune synapse genes was interrogated, we observed disproportionately hyper-methylated co-stimulatory genes and hypo-methylation of immune checkpoint genes, which were negatively associated with functional T-cell recruitment to the tumor microenvironment. Therefore, the methylation status of immune synapse genes reflects tumor immunogenicity and correlates with survival.

INTRODUCTION

Unprecedented clinical success with immune checkpoint inhibitors alludes to the pivotal importance of the immune synapse that forms between the antigen presenting cells and the effector T-cells (1). Professional antigen presenting cells such as dendritic cells present tumor-associated antigens via human leukocyte antigen complex (HLA) to the cognate T-cells to elicit tumor-specific immune responses (2). This high-fidelity recognition of tumor antigen by effector T-cells is either augmented by concomitant interaction of co-stimulatory molecules leading to a functional immune response, or interrupted by engagement of immune checkpoint molecules mediating T-cell anergy or exhaustion (2).

While professional antigen presenting cells are deemed critical for elicitation of a competent immune response, the immune synapse also forms between the tumor and the effector T-cells; thus, the tumor cells may evade the effector T-cells by neutralizing this interaction. In fact, the interaction between tumor cells and immune cells may shape the immune-suppressive landscape within the tumor microenvironment via mechanisms involved in downregulation of expression of both HLA and a wide array of immune checkpoint and co-stimulatory ligands to modulate T-cell responses (3). Indeed, the role of tumor in the immune synapse is best illustrated by a tendency of superior efficacy of PD1 blocking antibodies against tumors expressing high levels of PDL1 (4).

Expression of HLA and co-stimulatory/immune checkpoint molecules is intricately modulated at transcription, translation and post-translational levels (5). In particular, DNA methylation is a crucial epigenetic mechanism of immune regulation with critical roles in T-cell development and differentiation, antigen presentation, effector function and immunologic memory (6). Because cancer cells frequently utilize epigenetic dysregulation to silence tumor suppressors or activate oncogenes (7), we hypothesized that tumor progression requires epigenetic reprogramming of immune synapse genes to evade immune killing.

RESULTS AND DISCUSSIONS

Tumor evolution to evade immune-surveillance is a hallmark of carcinogenesis, and modulation of the immune synapse between antigen presenting cells and effector T-cells directly impacts tumor-specific immunity. As APCs and tumor modulate effector T-cells via ligands for co-stimulatory and immune checkpoint pathways, we focused on the methylation status of these ligands in tumor **(Figure 1A)**. The TCGA Level 1 methylation data from 30 solid tumor types were studied **(Table S1)**. Twenty selected genes were divided into two groups, immune checkpoint genes (ICG) and co-stimulatory genes (CSG), (**Table S2**). Of note, *CD80* and *CD86* have dual roles as both stimulatory when interacting with *CD28* or inhibitory as a ligand for CTLA-4. Prior studies suggest that their affinity is stronger for CTLA-4 and thus likely to mediate inhibitory signals when expressed in low levels, as is generally the case in tumors (8). Therefore, these two genes were categorized as inhibitory genes in the tumor-immune synapse.

We first investigated whether distinct tumor types were identifiable based on the methylation status of the immune synapse genes using two dimensional t-distributed stochastic neighbor embedding (t-SNE) (9) and unbiased hierarchical clustering analysis. Strikingly, patients with the same tumor type clustered together regardless of other clinical characteristics including age, sex or stage **(Figure 1B-D)**. This finding suggests the methylation status of immune synapse genes is heavily imprinted by the tissue of origin. By contrast, normal adjacent tissue of the same histology differentially segregated within the cluster highlighting the epigenetic evolution of tumors during carcinogenesis **(Figure 1B-D)**. For instance, breast cancer (inverted pink triangle) is clearly separated from its counterpart normal adjacent tissue.

Unbiased t-SNE and hierarchical clustering analysis demonstrated that the methylation status of immune synapse genes alone can distinguish tumor vs. normal tissue and histologic subtypes opening up an intriguing possibility that the methylation status of immune synapse genes may be utilized for early detection of cancer.

Next, we endeavored to understand the biologic basis of separation between the tumor and the normal adjacent tissue by the methylation status of ICG and CSG by analyzing the methylation pattern of individual genes and their CpG-probes on the 450K chip. A full list of the genes and their probes is given in Table S3. Recent studies have demonstrated that DNA methylation of gene bodies may also contribute to transcriptional regulation (10), however, the probes targeting the putative promoter region of the genes within TSS1500, TSS200, and 5'UTR were evaluated. Interestingly, ICGs and CSGs demonstrated inverse methylation patterns reflecting their opposite immunomodulatory functions **(Figure 2, S1-S16)**. For instance, the β-values of probes within the *CD40* gene locus, a prominent CSG, have demonstrated profound hypermethylation in the tumor while the *HHLA2* gene locus, an ICG, demonstrated hypomethylation in the tumor in comparison to the normal adjacent tissue **(Figure 2A)**. By contrast, the opposite phenomenon was observed for the CSG genes with an increased methylation in tumor vs. normal adjacent tissue **(Figure 2B)**. The correlation between probes within the same gene is high, indicating the consistence of the methylation level measurements (**Figure S1**). Because the known epigenetic mechanism of gene methylation is transcriptional suppression, we interrogated the relationship between the methylation status and its gene expression. As anticipated, an inverse correlation between methylation and gene expression was manifest among tumor and normal adjacent tissue **(Figure 2C-D)**. Such inverse relationship however was confined to tumor samples with detectable gene expression (i.e. log2 expression > 4) **(Figure 2D)**. The average methylation level was calculated using probes located in the TSS1500, TSS200 or 5'UTR region of the gene and with a r<-0.2 (**Table S3**). Importantly, the average β-value of the selected probes within the *HHLA2* and *CD40* gene loci demonstrated consistent methylation patterns across disease sites **(Figure 2E)**: hypermethylation of *CD40* and hypomethylation of *HHLA2* in comparison to the normal adjacent tissue. Additionally, for both

HHLA2 and *CD40*, the tumor samples demonstrated a larger variance in the methylation levels in tumor vs. normal tissue across disease sites **(Figure 2E)**.

These results suggest that the tumor-immune synapse is regulated at least in part by methylation in cancer. Sporadic evidence for regulation of *HLA* (11, 12), *CD40* (11), or *CD80* (13) by methylation in select tumor types now appears a more generalized phenomenon in the majority of co-stimulatory and immune checkpoint genes across tumor types. Interestingly, consistent with previous reports of PD-L1 promoter regulation by methylation (14), two probes within the promoter region were negatively correlated with the gene expression. However, a clear trend for hypomethylation of PD-L1 locus in comparison to normal adjacent tissue was not observed, suggesting competing mechanisms governing PD-L1 expression **(Figure S4)**.

Next, we conducted a principal component analysis (PCA) to summarize the methylation pattern across all genes and their CpG-probes. To minimize noise and enrich for biologically relevant signal, only the CSGs and ICGs CpG-probes that demonstrated negative correlation ($r<-0.2$) between the methylation status and their corresponding gene expression and located in the TSS1500, TSS200, 5'UTR regions were selected for further analysis; in total 75 probes. **(Figure 2, S1-S16, Table S3-S4)**. PCA revealed two major principal components, explaining 22.6% and 16.6% of the variation, respectively. A two-dimensional representation of PC1 and PC2 for 8,186 solid tumors and 745 normal adjacent tissues clearly showed that many tumors have an abnormal methylation pattern **(Figure 3A)**. Strikingly, the dominant components of PC1 were CSGs, in particular *CD40* and *HLA-A*. By contrast, PC2 was mainly driven by ICGs including *VTCN1*, *HHLA2*, *PDL1*, *CEACAM1*, *CD80*, and *CD86* **(Figure 3B, S17)**. Consequently, PC1 and PC2 were highly correlated with average β-values of CSG probes and ICG probes respectively **(Figure S17A-B)**. Probes from the same gene generally clustered together further confirming robustness of this analysis **(Figure 3B)**. It should be noted that all CpG-probes contribute to both PCA components with variable contributions, some with a negative weight for a specific PCA component. The total score for a sample will thus be a weighted average of all variables.

Consistent with the methylation patterns observed with individual CSG and ICG, primary tumor exhibited higher PC1 and lower PC2 scores in comparison to the normal adjacent tissue score across disease sites **(Figure 3C),** which was also replicated in the average β-values of CSG and ICG probes **(Figure S17D-E).** Importantly, we observed reversal of hypermethylation of CSGs by 5-azacytidine in the dataset of 26 epithelial cancer cell lines (15) with a significant decrease in PC1 scores **(Figure 3D)**. At an individual gene level, demethylation of *CD40* by azacytidine was also evident **(Figure 3E)** underscoring that the methylation status of CSGs is therapeutically actionable.

Two-dimensional evaluation of CSG and ICG methylation status revealed that normal tissues generally exhibit relative hyper-methylation of ICGs and hypomethylation of CSGs, demonstrating absence of epigenetic brake to suppress immune response. Indeed, highly efficient central tolerance mechanisms governing clonal deletion of self-reactive T-cells allows normal tissues to remain highly immunogenic to any abnormal presence of foreign antigens, which usually represent infection. By contrast, tumor tissues manifest either hypermethylation of CSGs and/or hypomethylation of ICGs, effectively employing epigenetic mechanisms to deliberately suppress the immune system. Because of neo-antigens, oncogenic viral antigens, or cancer testis antigens, tumor specific immune responses ensue. Therefore, altered methylation status may reflect tumor adaptation to evolutionary pressure exerted by immune-surveillance. Relatively consistent methylation phenotype between early stage and late stage melanoma suggests such epigenetic adaptation occurs early during carcinogenesis, which explains in part the markedly consistent methylation phenotype of immune synapse genes across tumor types. While expression of HLA and co-stimulatory/immune checkpoint molecules is frequently dysregulated in cancer via multiple mechanisms (11), heritable changes to impact the entire tumor tissue as a whole require the initial cascade of tolerogenic signal to involve genetic or epigenetic changes. Because germline or somatic mutations of these immune synapse genes are rare events (12), the immune status of tumor manifest on the epigenetic footprints of immune synapse genes.

Because immune evasion is critical for cancer progression and survival, we hypothesized that the differential methylation status of the immune synapse genes may determine clinical outcome. Therefore, we investigated the clinical relevance of our PCA model in melanoma, a prototypic immunogenic cancer. PC1 was a determinant of disease specific survival (DSS) in melanoma with significant survival advantage in $PC1^{low}$ patients characterized by hypomethylation of CSGs **(Figure 4A)**. An alternate approach with partial least squares (PLS) modeling using the outcome as response variable also confirmed differences in survival outcome based on CSGs **(Figure S18)**. Interestingly, the PC1 score was relatively consistent among early and late stage melanoma patients, and thus, the survival difference was independent of patient staging **(Figure 4B)**.

The methylation status of immune synapse genes was prognostic only in immunogenic tumors suggesting that modulation of tumor-immune synapse by methylation may become clinically relevant only in the presence of active anti-tumor immune responses. For instance, PC1 was prognostic for DSS in uterine corpus endometrial carcinoma (UCEC) with microsatellite instability (MSI-H) **(Figure 4C)**. By contrast, no differences in survival was noted based on PC1 in UCEC without MSI (WT) **(Figure 4D)**. Consistently, the methylation status correlated with overall survival (OS) and DSS also in other relatively immunogenic cancers, including non-small cell lung cancer (NSCLC), renal cell carcinoma (RCC) and head and neck cancer (HNSC). Similar to our findings with melanoma, NSCLC patients with lower PC1 score demonstrated improved survival **(Figure S19)**. By contrast, prognosis for head and neck squamous cell carcinoma and renal cell carcinoma correlated with PC2 **(Figure S20).**

Increased tumor infiltration by $CD4^+$ and $CD8^+$ T-cells was evident in $PC1^{low}$ patients **(Figure 4E)**. Further, increased levels of CD3ζ (*CD247*), Granzyme B (*GZMB*), Perforin (*PRF1*), and IFNγ in $PC1^{low}$ patients suggest superior effector functions by these T-cells **(Figure 4F)**. Interestingly, key chemokines that drive T-cell recruitment and trafficking in melanoma (16),

CCL2, *CCL3*, *CCL4*, *CCL5*, *CXCL9*, and *CXCL10*, were elevated in $PC1^{low}$ patients **(Figure 4G)**. More recently, STING/cGAS pathway has been critically implicated in tumor immunogenicity. A significant increase in *cGAS* expression was also manifest in $PC1^{low}$ patients **(Figure 4H)**. Therefore, hypomethylation of CSGs in melanoma was associated with improved survival as well as enhanced tumor immunogenicity and recruitment of effector T-cells.

In summary, we report methylation of immune synapse genes as a crucial driver of tolerogenic immune landscapes in cancer. Notably, preclinical studies have demonstrated the efficacy of demethylating agents to augment immunotherapy (17, 18). Based on our study, we predict the subset of patients with hypermethylated CSGs ($PC1^{high}$) may benefit from combination therapy of PD1 blockade with 5-azacitidine, while conversely, patients with hypermethylated ICGs ($PC2^{high}$) may be adversely impacted. Given negative preliminary findings from the phase II randomized clinical trial of oral 5-azacitidine plus pembrolizumab vs pembrolizumab plus placebo (19), patient selection may be crucial to overcome resistance to PD1 blockade. Alternatively, targeted editing of tumor methylation of immune synapse genes by TET1 or DNMT3a via CRISPR may allow personalized approach to augment immunotherapy (20). Notably, the methylation status of immune synapse genes may be utilized to predict response to immunotherapy. The major advantage to the use of the methylation status is that DNA is stable and degradation is less likely in Formalin-Fixed Paraffin-Embedded tissues, and thus anticipated to be more robust than RNA based or histology based approaches.

METHODS

Analysis of TCGA methylation database

TCGA Level 1 IDAT files for the selected tumor types was downloaded between April and May of 2016 using the former (now defunct) Data Matrix accessed through http://tcga-data.nci.nih.gov/tcga/dataAccessMatrix.htm. Preprocessing the data included normalization via internal controls probe followed by background subtraction using the methylumi R package from Bioconductor (21). The calculated β-values were then extracted from the MethyLumiSet object following preprocessing.

Analysis of TCGA RNAseq database

The TCGA RNAseq samples was extracted from the "EBPlusPlusAdjustPANCAN_IlluminaHiSeq_RNASeqV2.geneExp.tsv" file available from: https://gdc.cancer.gov/about-data/publications/pancanatlas and log2 transformed, log2(x+1).

GSE57342 5-azacitidine treated cancer cell lines

The GSE57342 processed dataset was downloaded and cell lines with more than three Mock- and three 5-azacitidine-treated samples was selected for analysis.

T-SNE analysis

T-SNE was calculated using all 247 probes for the selected 20 genes across all TCGA samples. The 50 first PCA-components was used as input with perplexity=50 and Euclidian distance as implemented in MATLAB.

Correlation coefficient heatmap

The Pearson's correlation coefficients between all the probes within a gene were calculated and displayed as a heatmap.

Principal component analysis

We used the first and second principal component (a weighted average β-values among the CSG and ICG probes), as they account for the largest variability in the data, to represent the

overall methylation status for 8,931 tumor and normal samples in the TCGA database. That is, PC = $\Sigma w_i x_i$, a weighted average β-values among the selected CSG and ICG probes, where *xi* represents gene *i* β-value, w_i is the corresponding weight (loading coefficient) with $\Sigma w_i^2 = 1$, and the w_i values maximize the variance of $\Sigma w_i x_i$. For each gene, a set of probes were selected using the following criteria to minimize noise, r<-0.2 (methylation vs gene expression) located in the TSS1500, TSS200 or the 5'UTR **(Table S4)**. Each probe was centered but not scaled before PCA calculations.

Survival analysis

OS and DSS, was retrieved from the prior publication (5). Tertiles were used to define high, intermediate (Int) and low PC1 or PC2 for melanoma, NSCLC, HNSC, RCC, UCEC MSI^{hi} and wild type patients. Kaplan-Meier curves were then plotted based on tertile scores.

Partial Least Squares (PLS) modelling

A PLS model was derived using melanoma poor survivors (DSS Dead<12 months, 0) and long survivors (DSS Alive>120 months, 1) as a binary response using the CSG-probes. Cross validation indicated two significant PLS components. The PLS model was then applied to the melanoma samples *not* used in training. Samples with a predicted response>0.5 was compared to samples with a predicted response<0.5 using a log rank test.

MSI status

The MSI status was extracted from Bonneville et al (22). Samples with a MANTIS score larger than 0.4 was considered MSI positive as described in the publication.

Statistics

T-SNE, PCA, PLS, Pearson and Spearman correlation statistics, and two-sided Student's t-tests were done in MATLAB R2018B. Survival analysis was done using MatSurv.

Study approval

Only publicly available, deidentified data are presented; thus, institutional study approval was not required.

AUTHOR CONTRIBUTIONS: A.B performed bioinformatics analyses and created figures; R.M.P downloaded and processes the methylation data, M.M and S.K curated clinical data; I.H contributed to generating figures; AB, J.M and S.K analyzed and interpreted the data.

ACKNOWLEDGMENTS: The authors acknowledge Dr. Conejo-Garcia for discussions. This work was supported by K08 CA194273, Immunology Innovation Fund, NCI Cancer Center Support Grant (P30-CA076292), the Miriam and Sheldon G. Adelson Foundation, and the Moffitt Foundation.

REFERENCE

1. Pardoll DM. The blockade of immune checkpoints in cancer immunotherapy. *Nature reviews.* 2012;12(4):252-64.
2. Chen L, and Flies DB. Molecular mechanisms of T cell co-stimulation and co-inhibition. *Nature reviews Immunology.* 2013;13(4):227-42.
3. Sade-Feldman M, Jiao YJ, Chen JH, Rooney MS, Barzily-Rokni M, Eliane JP, et al. Resistance to checkpoint blockade therapy through inactivation of antigen presentation. *Nature communications.* 2017;8(1):1136.
4. Kluger HM, Zito CR, Turcu G, Baine MK, Zhang H, Adeniran A, et al. PD-L1 Studies Across Tumor Types, Its Differential Expression and Predictive Value in Patients Treated with Immune Checkpoint Inhibitors. *Clinical cancer research : an official journal of the American Association for Cancer Research.* 2017;23(15):4270-9.
5. Thorsson V, Gibbs DL, Brown SD, Wolf D, Bortone DS, Ou Yang TH, et al. The Immune Landscape of Cancer. *Immunity.* 2018;48(4):812-30 e14.
6. Fitzpatrick DR, and Wilson CB. Methylation and demethylation in the regulation of genes, cells, and responses in the immune system. *Clin Immunol.* 2003;109(1):37-45.
7. Ehrlich M. DNA methylation and cancer-associated genetic instability. *Adv Exp Med Biol.* 2005;570:363-92.
8. Tirapu I, Huarte E, Guiducci C, Arina A, Zaratiegui M, Murillo O, et al. Low surface expression of B7-1 (CD80) is an immunoescape mechanism of colon carcinoma. *Cancer Res.* 2006;66(4):2442-50.
9. Van der Maaten L. Visualizing Data using t-SNE. *Journal of Machine Learning Research.* 2008;9:2579-605.
10. Suzuki MM, and Bird A. DNA methylation landscapes: provocative insights from epigenomics. *Nature reviews Genetics.* 2008;9(6):465-76.
11. Micevic G, Thakral D, McGeary M, and Bosenberg M. PD-L1 methylation regulates PD-L1 expression and is associated with melanoma survival. *Pigment cell & melanoma research.* 2018.
12. Serrano A, Tanzarella S, Lionello I, Mendez R, Traversari C, Ruiz-Cabello F, et al. Rexpression of HLA class I antigens and restoration of antigen-specific CTL response in melanoma cells following 5-aza-2'-deoxycytidine treatment. *International journal of cancer Journal international du cancer.* 2001;94(2):243-51.
13. Scarpa M, Scarpa M, Castagliuolo I, Erroi F, Basato S, Brun P, et al. CD80 down-regulation is associated to aberrant DNA methylation in non-inflammatory colon carcinogenesis. *BMC cancer.* 2016;16:388.
14. Kowanetz M, Zou W, Gettinger SN, Koeppen H, Kockx M, Schmid P, et al. Differential regulation of PD-L1 expression by immune and tumor cells in NSCLC and the response to treatment with atezolizumab (anti-PD-L1). *Proc Natl Acad Sci U S A.* 2018;115(43):E10119-E26.
15. Li H, Chiappinelli KB, Guzzetta AA, Easwaran H, Yen RW, Vatapalli R, et al. Immune regulation by low doses of the DNA methyltransferase inhibitor 5-azacitidine in common human epithelial cancers. *Oncotarget.* 2014;5(3):587-98.
16. Harlin H, Meng Y, Peterson AC, Zha Y, Tretiakova M, Slingluff C, et al. Chemokine expression in melanoma metastases associated with CD8+ T-cell recruitment. *Cancer Res.* 2009;69(7):3077-85.

17. Wrangle J, Wang W, Koch A, Easwaran H, Mohammad HP, Vendetti F, et al. Alterations of immune response of Non-Small Cell Lung Cancer with Azacytidine. *Oncotarget.* 2013;4(11):2067-79.
18. Chiappinelli KB, Strissel PL, Desrichard A, Li H, Henke C, Akman B, et al. Inhibiting DNA Methylation Causes an Interferon Response in Cancer via dsRNA Including Endogenous Retroviruses. *Cell.* 2017;169(2):361.
19. Levy BP, Giaccone G, Besse B, Felip E, Garassino MC, Domine Gomez M, et al. Randomised phase 2 study of pembrolizumab plus CC-486 versus pembrolizumab plus placebo in patients with previously treated advanced non-small cell lung cancer. *European journal of cancer.* 2019;108:120-8.
20. Liu XS, Wu H, Ji X, Stelzer Y, Wu X, Czauderna S, et al. Editing DNA Methylation in the Mammalian Genome. *Cell.* 2016;167(1):233-47 e17.
21. Davis S DP, Bilke S, Triche T, Bootwalla M. Handle Illumina methylation data. R package version 2.12.0. 2014.
22. Bonneville R, Krook MA, Kautto EA, Miya J, Wing MR, Chen HZ, et al. Landscape of Microsatellite Instability Across 39 Cancer Types. *JCO precision oncology.* 2017;2017.

FIGURES AND FIGURE LEGENDS

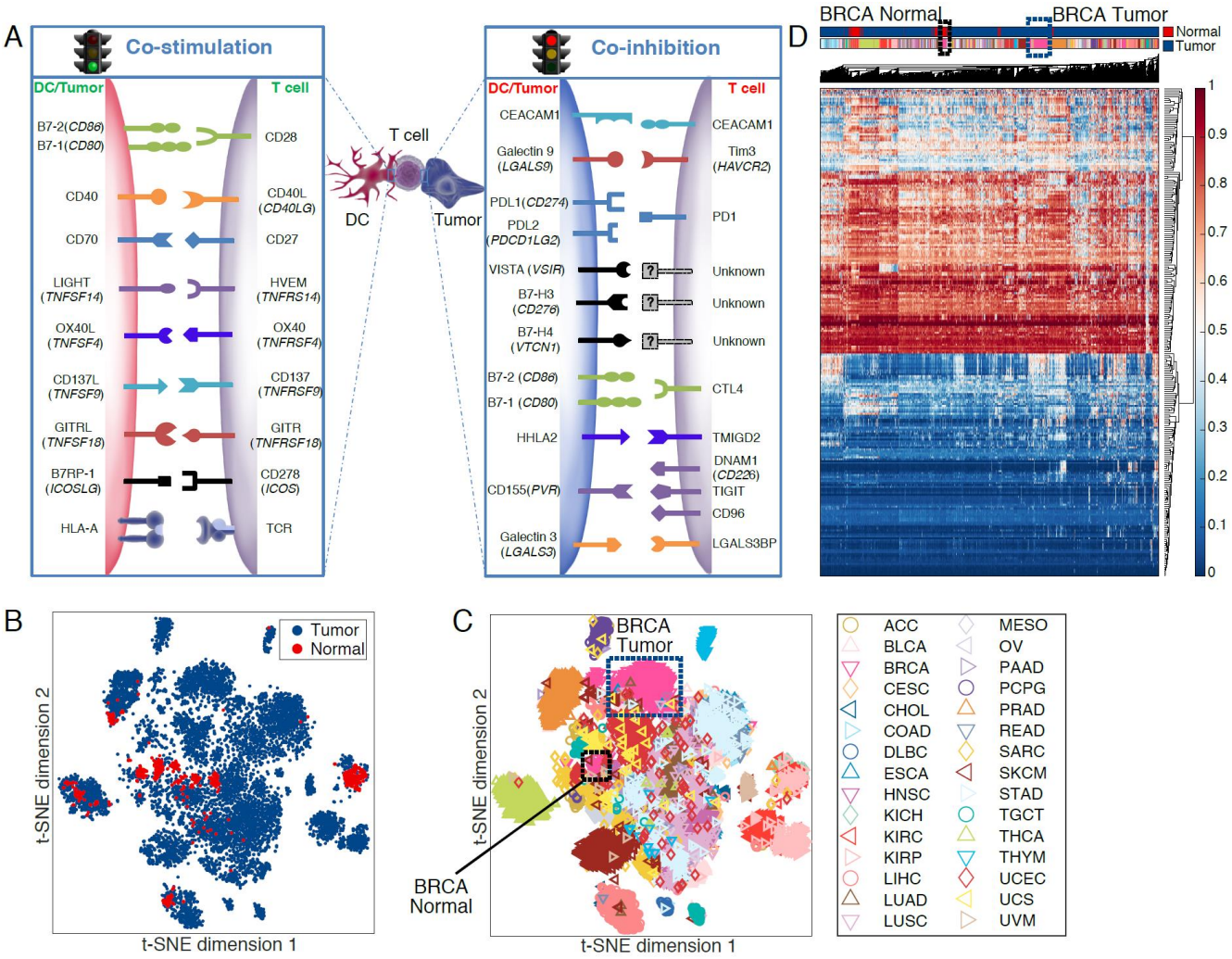

Figure 1. The distinct pattern of immune synapse gene methylation depends on tumor histology. (A) The schematic of immune synapse between the antigen presenting cells/tumor and T-cells is demonstrated. (B) T-SNE analysis was performed on 8,186 solid tumors and 745 normal adjacent tissues based on the β-values for methylation levels on all probes for CSGs and ICGs from (A) contrasting tumor (blue) vs. normal adjacent tissue (red). (C) The spatial relationship between distinct tumor types is depicted with breast tumors in blue- and normal adjacent tissue samples black-dotted boxes. (D) Unbiased hierarchical clustering analysis is shown.

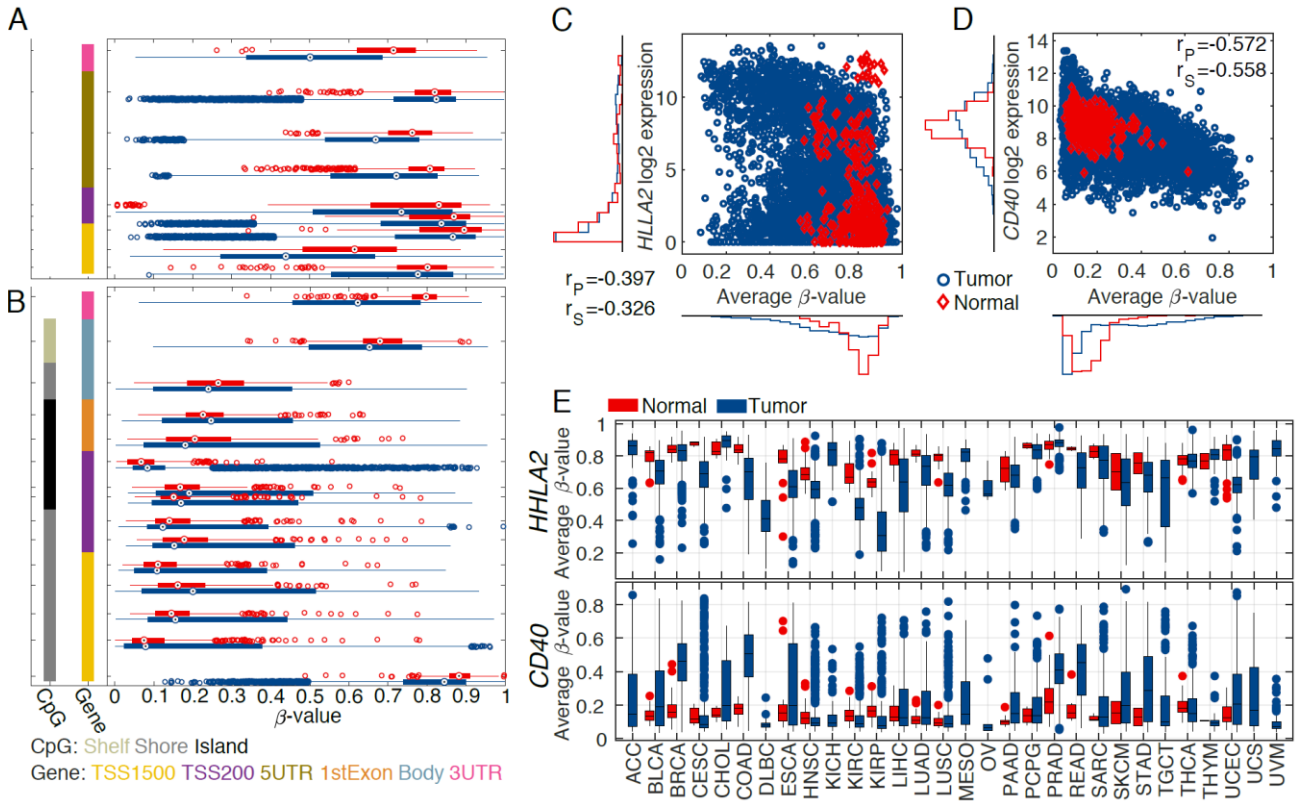

Figure 2. The polarity of methylation patterns for co-stimulatory and immune checkpoint ligands. (A, B) β-values of methylation probes for TSS1500, TSS200, 5'UTR, body, and 3'UTR of *HHLA2* gene (A), an example of ICG, or *CD40* (B), an example of CSG, derived from all tumor samples (blue) and normal adjacent tissues (red) are depicted. The methylation level for each probe is represented by a box-plot. The left most column indicates the presence of CpG-island, while the second column colors indicate where on the gene the probe is located. The average β-values for selected probes within TSS1500, TSS200, and 5'UTR are plotted against gene expression for *HHLA2* (C) or *CD40* (D). Each circle represents an individual tissue sample. (E) A box plot of average β-values for selected probes *HHLA2* and *CD40* from tumor (blue) and normal adjacent tissue (red) are shown. R_P and R_S are Pearson and Spearman correlation coefficient respectively.

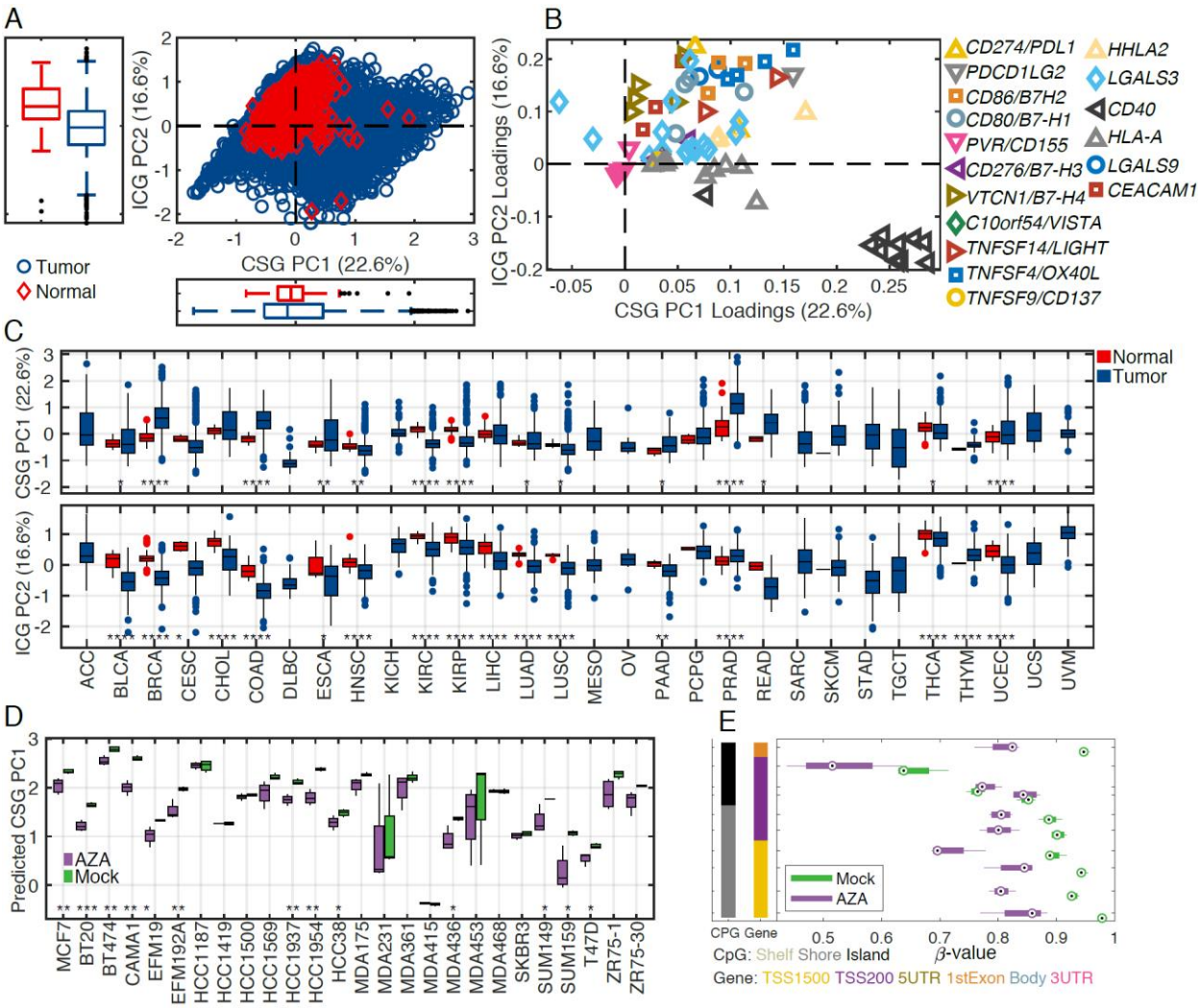

Figure 3. Principal component analysis (PCA) segregates co-stimulatory and immune checkpoint ligands. (A) Two-dimensional plot of PC1 and PC2 scores for all tumor types (blue) and normal adjacent tissues (red) is shown. (B) The importance of each variable, CpG-probes, for PC1 and PC2 are depicted. (C) A box plot of PC1 and PC2 scores for tumor (blue) and normal adjacent tissue (red) compared across histologic types. (D) PC1 scores of mock- or 5-azacitidine-treated epithelial cancer cell lines. (E) The methylation status of CD40 gene in mock- or azacytidine-treated CAMA1 cell line. * p<0.05, ** p<0.01, *** p<0.001, **** p<0.0001 by t-test.

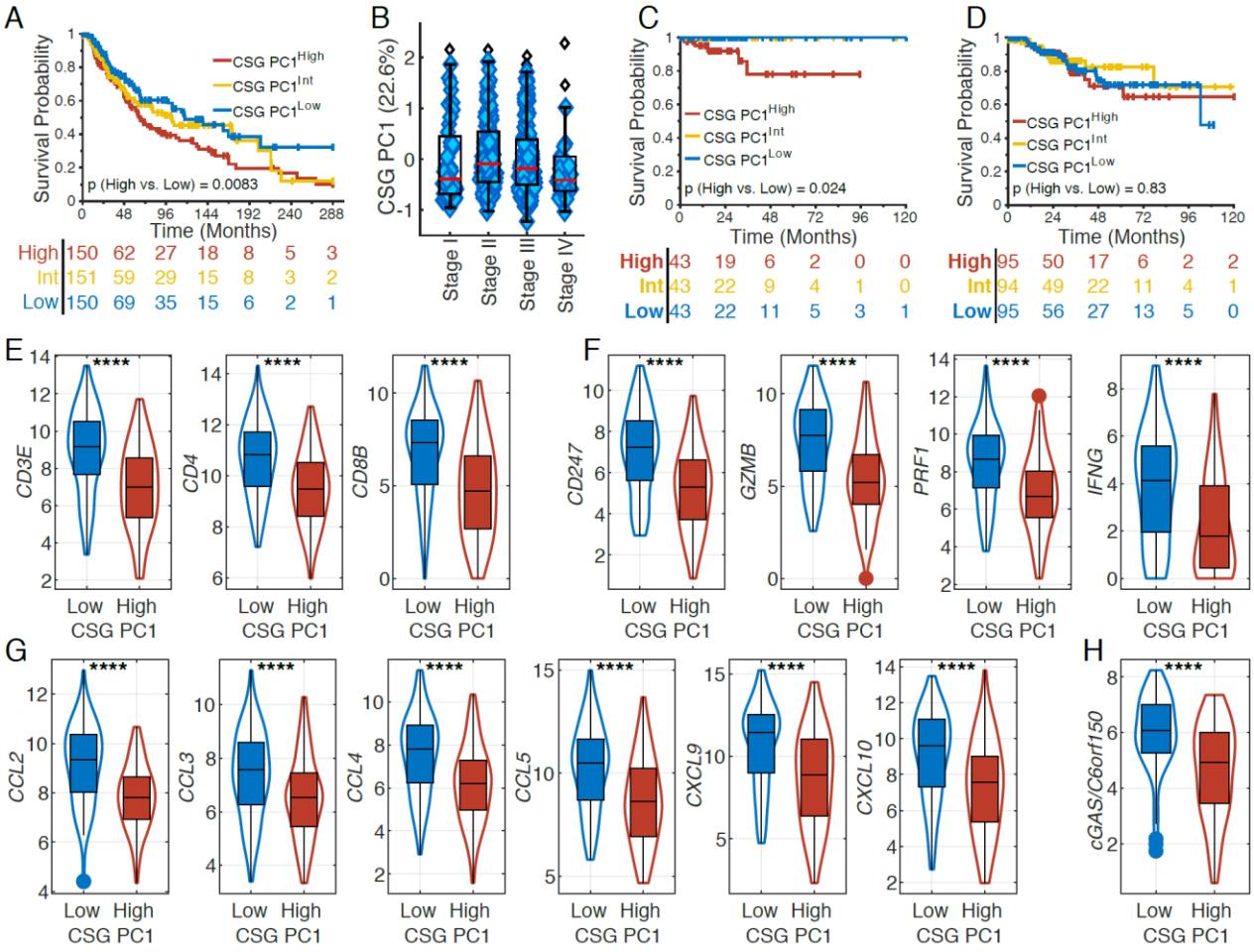

Figure 4. The methylation status of co-stimulatory ligands is prognostic in melanoma. (A) Kaplan-Meier curves for DSS of melanoma patients with high, intermediate, and low tertials of PC1 score are shown. Higher PC1 score represents hypermethylation of CSGs. (B) Box-plot of PC1 score distribution based on melanoma patient staging. (C, D) Kaplan-Meier curves for DSS of UCEC patients with MSI (C) or without MSI (D) with high, intermediate, and low tertiles of PC1 score are shown. (E) T-cell recruitment in $PC1^{high}$ and $PC1^{low}$ melanoma patients is approximated by gene expression of *CD3E*, *CD4* and *CD8B*. (F) T effector functions in $PC1^{high}$ and $PC1^{low}$ melanoma patients is approximated by gene expression of *CD3ζ* (*CD247*), Granzyme B (*GZMB*), Perforin (*PRF1*), and IFNγ. (G) Chemokines for immune cell trafficking in $PC1^{high}$ and $PC1^{low}$ melanoma patients is approximated by gene expression of *CCL2*, *CCL3*, *CCL4*, *CCL5*, *CXCL9* and *CXCL10*. (H) Immunogenicity of $PC1^{high}$ and $PC1^{low}$ melanoma patients is approximated by gene expression of *cGAS*. p-value in panel A, C and D is a log rank test between High and Low group. ****, p<0.0001 by t-test.